

International Conference on Space Optics—ICSO 2012

Ajaccio, Corse

9–12 October 2012

Edited by Bruno Cugny, Errico Armandillo, and Nikos Karafolas



Wide angle light scattering and complex optical filters: modelization and characterization

Myriam Zerrad

Michel Lequime

Claude Amra



Wide angle light scattering & Complex Optical filters: Modelization and Characterization

Myriam Zerrad, Michel Lequime and Claude Amra

Institut Fresnel

CNRSTI UMR 6133, Aix-Marseille Universités, Ecole Centrale Marseille,

D.U. St Jérôme 13397 Marseille Cedex 20, France

myriam.zerrad@fresnel.fr

Abstract — Because of their complexity (>100 layers) and their decreasing dimensions (~pixel size), performances of the new generation of optical filters for space application are degraded by wide angle light scattering. For these reasons, it is huge important to be able to predict and measure the angular and spectral behaviour of light scattered by complex interferential filters. In this paper, light scattering is calculated for complex filters and take simultaneously account of most parameters: surface roughness, bulk inhomogeneity, cross-correlation coefficients, errors in design, wavelength and scattering angles (normal and polar), polarization... All these variations have become necessary to predict a balance in optical multiplexers and related systems, mainly for space applications. To complete the analysis, a metrological platform dedicated to the multimodal characterization of scattering losses has been involved.

Index Terms — Light scattering, spectral scattering, 3D scattering, roughness, optical coatings metrology, polarization & scattering, speckle, contamination

I. INTRODUCTION

Light scattering in optical coatings has been the focus of numerous studies for decades. Indeed in a way similar to absorption, scattering has driven the performances of the most complex interferential filters. The origins of scattering can be found in roughness at the stack interfaces and bulk inhomogeneities in the film bulks. It was well established that all these defects include the replication of the substrate roughness at each interface, as well pits due to the deposition process and localized defects resulting from dusts. Moreover, a residual roughness can be introduced in relationship with the thin film material grain size.

Most difficulties have been considerably reduced in the 2000's, and are mainly due to the improvement of cleaning and polishing processes, together with deposition technologies and monitoring processes. However these new technologies today allow to deposit a much higher number of layers and a new complexity has increased in consequence. Within this framework scattering phenomena must again be investigated with more detail, including spectral, angular and polar variations resulting from each illuminated pixel on the surface sample.

Due to new computer performances, light scattering can be easily calculated for complex filters and take simultaneously account of most parameters: surface roughness, bulk inhomogeneity, cross-correlation coefficients, errors in design, wavelength and scattering angles (normal and polar), polarization... All these variations have become necessary to predict a balance in optical multiplexers and related systems, mainly for space applications.

Some examples are given in the figures further, with a special focus on polar and spectral variations, that emphasize the complexity of the process.

In order to face such huge collection of data, it has become more and more necessary to have at disposal a facility able to measure the same information. For this reason new developments were performed in Marseille these last years, that we will first recall. Then we show how to extend these facilities and try to reach a multimodal scatterometer..

II. LIGHT SCATTERING AND OPTICAL MULTILAYERS: NUMERICAL TOOLS

Based on first order vector theory, the electromagnetic field scattered by a multilayer can be calculated as a function of the stack formula, the illumination conditions (optical term C), the microstructure of the component (γ is representative of the interfaces roughness or the bulk inhomogeneities in the layers). The expression of the intensity of the light scattered by an optical multilayer is given eq(1) as a function of the scattering angles (θ, ϕ) defined Figure 1, the illumination wavelength (λ) and angle (i). In eq (1), p and q are indexing the layer #, h_p is the profile of interface # p , \hat{h}_p its Fourier transform, δ_p its rms roughness and γ_p its roughness spectrum or permittivity spectrum.

$$I(\vec{\sigma}, \lambda, i) = \sum_{p \neq q} C_{pq}(\vec{\sigma}, \lambda, i) \alpha_{pq}(\vec{\sigma}, \lambda, i) \gamma_p(\vec{\sigma}, \lambda, i) \quad (1)$$

With
$$\gamma_p(\vec{\sigma}) = \frac{4\pi^2}{S} |\hat{h}_p(\vec{\sigma})|^2 \quad (2)$$

And
$$\delta_p^2 = \int_{\vec{\sigma}} \gamma_p(\vec{\sigma}) d\vec{\sigma} \quad (3)$$

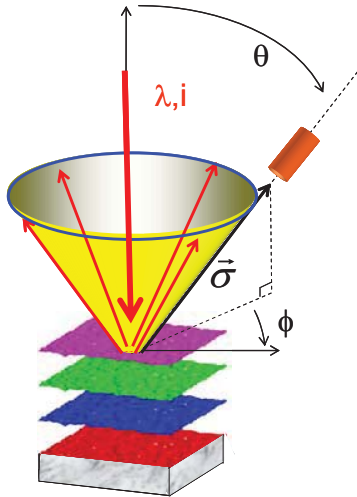


Figure 1 : light scattering by optical components: definition of scattering angles (θ, ϕ)

As an illustration, the *BRDF* (Bidirectional Reflectance Distribution Pattern) calculated for a complex optical filter (91 layers self blocking filter) as a function of the normal scattering angle θ , in the incidence plane $\phi = 0^\circ$ and $\lambda = 740 \text{ nm}$ is given Figure 2.

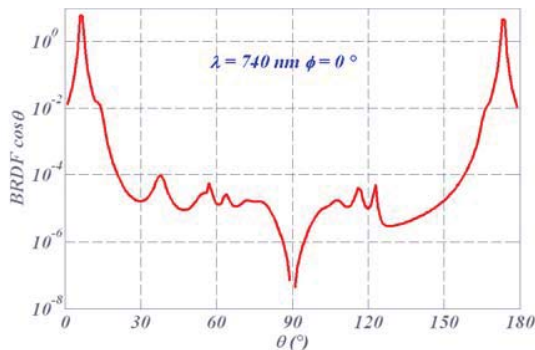


Figure 2: Theoretical *BRDF* calculated for a complex optical filter (91 layers self blocking filter) as a function of the normal scattering angle θ , at $\phi = 0^\circ$, for an illumination at $\lambda = 740 \text{ nm}$. Incidence angle is 10° .

For the characterization of optical coatings, the illumination wavelength has to be taken into account. As an example, we plotted in Figure 3 the spectral and angular variations of the intensity of the light scattered by a single-cavity Fabry Perot filter. As usual, the scattering rings appear in the spectral band-pass.

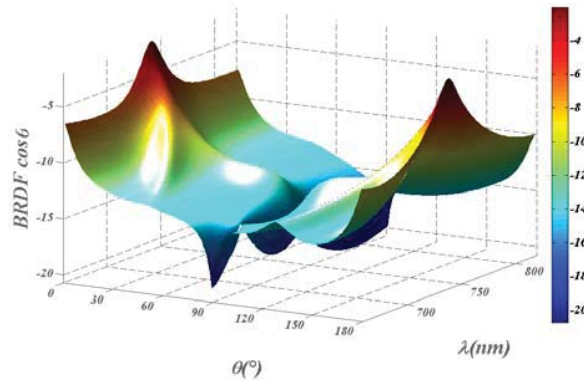


Figure 3: Theoretical *BRDF* calculated for a single-cavity Fabry Perot filter as a function of the normal scattering angle θ and illumination wavelength λ , at $\phi = 0^\circ$

Progress made in the last few years by technical deposition processes now allows to produce optical filters with much higher complexity (Figure 4), which increases the difficulty when analyzing such filters.

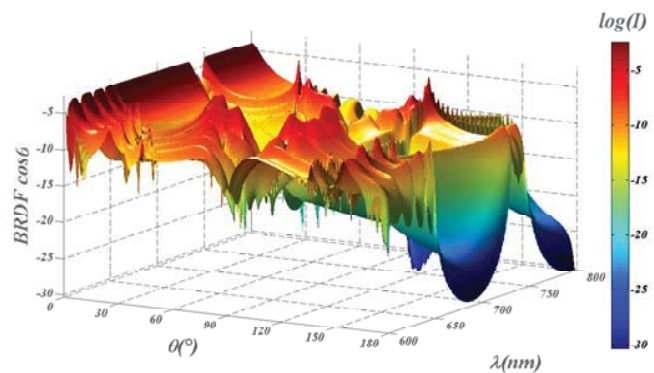


Figure 4 : spectral and angular variations of the light scattered by a 91 layers self blocking filter

Moreover, as shown on Figure 5, the 3D spatial repartition of the angular resolved scattering pattern (ARS) under normal incidence follows a polar symmetry. Fewer results can be found for polar dependence at oblique illumination, results that are given in figure 6.

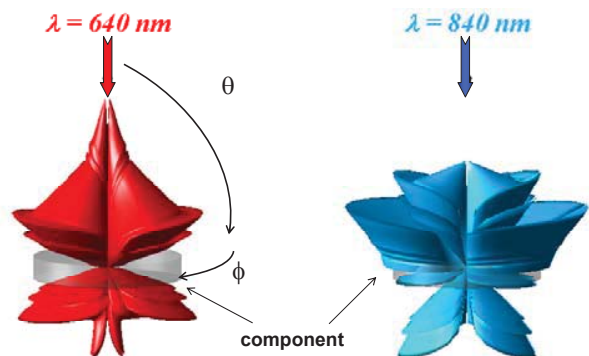


Figure 5: 3D spatial variations of the light scattered by a 91 layers self blocking filter at $\lambda = 640 \text{ nm}$ and $\lambda = 840 \text{ nm}$ under normal incidence

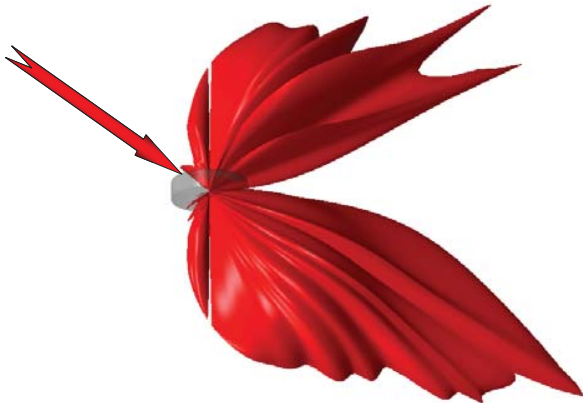


Figure 6: 3D spatial variations of the light scattered by a coating designed for total absorption and maximum field enhancement at total internal reflection

As illustrated on these numerical results, numerous parameters have to be taken into account for a comprehensive light scattering characterization of optical components. But, in term of experiment, they cannot be considered with the same accuracy at the same time, so it has been necessary to involve new facilities which now constitute a metrological platform dedicated to light scattering characterization.

III MULTI-WAVELENGTH 3D ARS SET-UP

A multi-wavelength 3D ARS set-up (Figure 7) located in a clean room allows the measurement of 3D scattering patterns at a wavelength which may be chosen between laser rays within [458 nm ; 10.6 μm].



Figure 7: 3D scatterometer

The signature of the instrument in the incident plane for an illumination wavelength of 633 nm is given Figure 8.

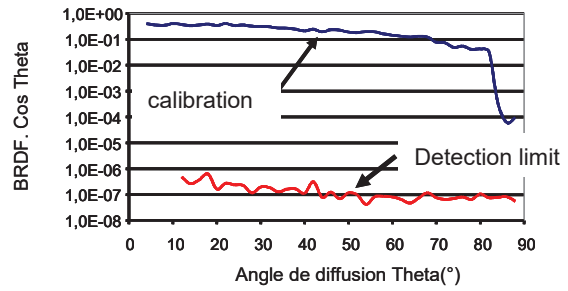


Figure 8: Signature of the 3D scatterometer @λ =633nm and φ=0°

Thanks to a high sensitivity CCD-array, measurements performed with extremely high angular resolution allow the recording of speckle intensity cartographies as shown on Figure 9-right. Statistical repartition of the speckle intensity extracted from only one intensity measurement allows discriminating the scattering origins as shown on Figure 9-left.

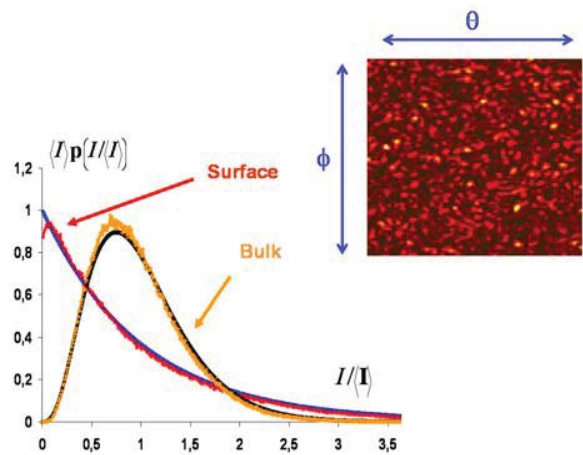


Figure 9: Speckle cartography and intensities histograms to discriminate scattering origin

To go further, the polarisation state of the incident light can be modulated and the recording of the polarimetric phase shift of the light scattered by the illuminated component allows a complementary discrimination of the scattering origin as illustrated on Figure 10.

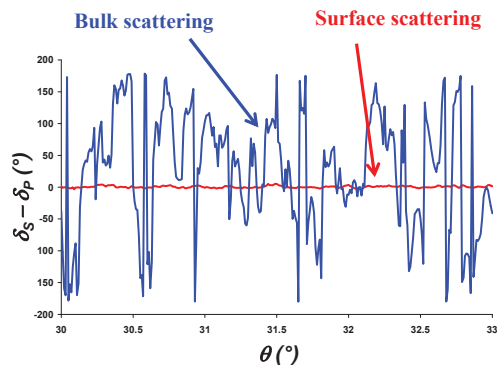


Figure 10 : Polarimetric phase shift of the light scattered by two lambertian scatterers

Moreover, polarisation state of the scattered wave can be measured with a resolution better than the speckle size. Under polarized illumination, the repartition of these polarization states can be related to the roughness and the mean slope of the illuminated surface. Figure 11 illustrates the numerical modelisation of the repartition of the polarization states of light scattered by different surfaces with rms roughnesses h_{rms} .

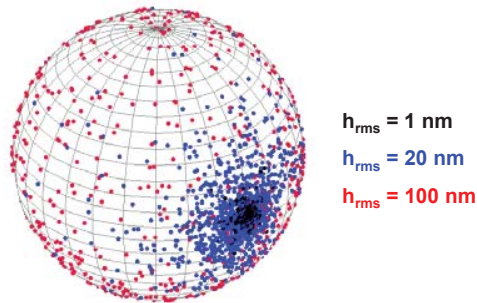


Figure 11: For 3 different rms roughness (1, 20 et 100 nm) surfaces, repartition on the Poincaré sphere of the polarization states of the scattered field for $\theta \in [10^\circ, 11^\circ]$

IV CCD-ARS SET UP: TO EXTRACT THE INFLUENCE OF LOCALIZED DEFECTS

One of the main problematic in light scattering characterization is the influence of defects localised on the sample surface. As illustrated Figure 12, only a few defects located on the illuminated area can modify significantly the shape and the level of the ARS pattern generated by the illuminated surface. As a consequence, if a surface whose intrinsic roughness is 0.87 nm is considered, the presence of only 10 localised defects on the sample will lead to the recording of a 3.93 nm by light scattering characterization.

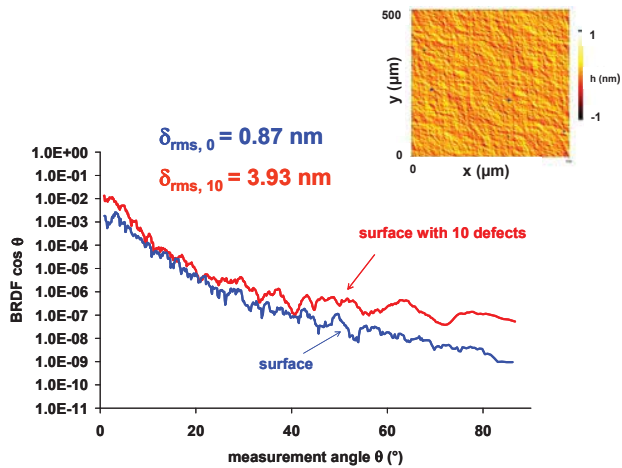


Figure 12: BRDF patterns @ $\lambda = 840$ nm calculated with first order theory from the surface profile given here (right) without defects (blue) and with 10 defects (red). Roughness are calculated from the corresponding scattering angular patterns

The previous example showed us that the influence of localized defects cannot be neglected in light scattering

characterization, so a dedicated set up was involved. The CCD-ARS set up is a goniometric light scattering instrument with high-resolution imaging. A schematic view of the set-up is given Figure 13 and the instrument signature can be seen Figure 14.

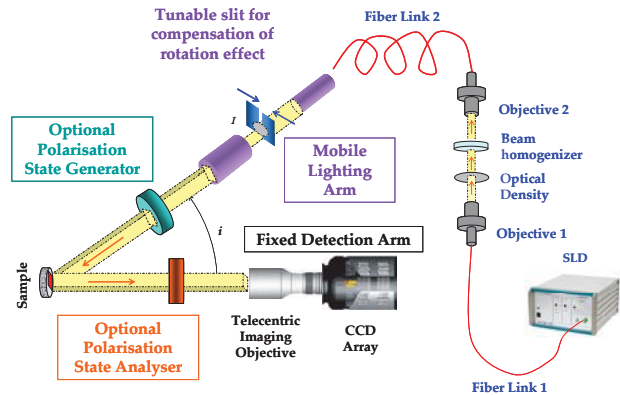


Figure 13: Schematic view of the CCD-ARS set up

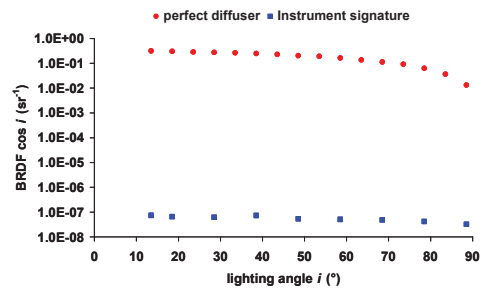


Figure 14 : CCD-ARS set up and the measured instrument signature

The illumination system is rotating around the sample surface and the area illuminated on the component is a 15.9x15.9 mm² square. For each lighting angle, the illuminated area is imaged with a very high-sensitivity CCD-array and a telecentric objective. The studied area is divided in more than 700 000 elementary 26μm x 26μm surfaces and the BRDF pattern of each of them is recorded at the same time. You can see Figure 15 an example of measurement performed on a contaminated Germanium wafer. Three BRDF patterns are plotted. First one (in red) is for an elementary surface free of defect, so, representative of the intrinsic roughness. Second one (in blue) is for an elementary surface with a defect (blue), so

the corresponding angular pattern presents some oscillations which are representative of the defect. And third one (green) is representative of the scattering level of a 2x2mm² square without localization of the defects and as a consequence is representative of the BRDF pattern which would have been recorded with standard ARS set-up. This example is illustrating the fact that compared to a classical BRDF measurement (green curve), the scattering pattern measured with the CCD-ARS set up is representative of the intrinsic roughness of the surface (red curve) or obviously show the presence of a defect (blue curve).

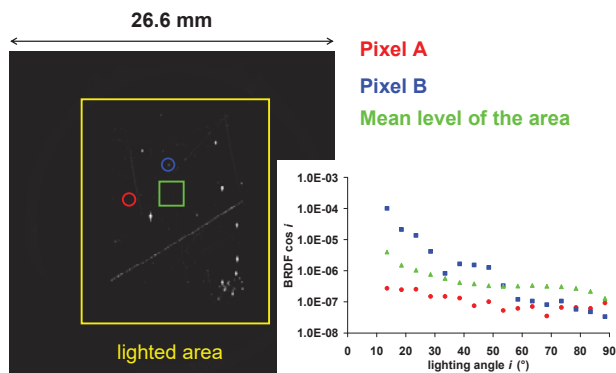


Figure 15: A germanium wafer imaged with the CCD-ARS set up and BRDF patterns of selected pixels (pixel A: without a defect; Pixel B: with a single defect; Test area : 2x2 mm² square area)

To extract from the spatially resolved BRDF measurement an accurate localisation of the defects on the surface, dedicated algorithms were involved. An example of application to the measurement shown Figure 15 is given Figure 16 where we can see the cartography of the local roughness measured on the sample with a spatially resolved ARS pattern measurement and after extraction of the pixels for which the signal recorded was affected by the presence of a defect.

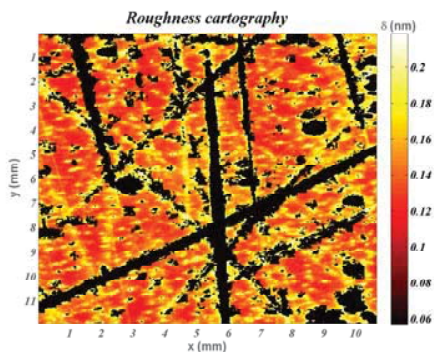


Figure 16 : roughness cartography after extraction of areas of influence of localized defects

Thanks to the huge number of resulting data, the statistical repartition of local roughness can be studied. An example of application is given Figure 17.

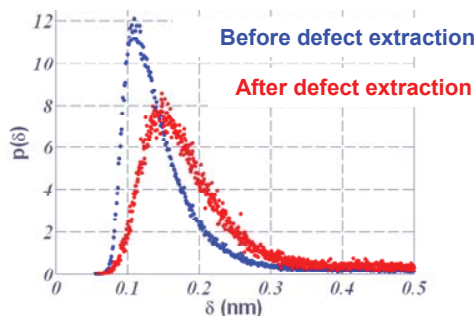


Figure 17 : Statistical repartition of the local roughness measured on the surface before and after extraction of the pixels whose measurement was disturbed by the vicinity of a defect

At last, as shown on Figure 13, we can add a polarization state generator and analyzer to the CCD-ARS set up. Such a new configuration allows us to record for each lighting angle, the Mueller matrix of the sample surface. The study of the polarimetric state of the light scattered by the component can give us complementary information on the nature of the defects. For example, we can see Figure 18, in the red circles the identification of 2 localized defects which have two different polarimetric behaviors. And this shows us that these two defects are not from the same material. So the use of the spatially resolved Mueller imaging allows the discrimination between different kind of defects.

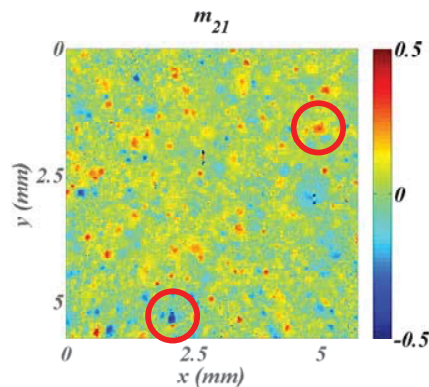


Figure 18: Cartography of the Mueller matrix coefficient m_{21} measured on dielectric quarter-wave mirror centered @ $\lambda = 633$ nm with a 60° illumination angle.

To go further and to reach a comprehensive light scattering characterization, as shown in part II, it is necessary to take into account the spectral effects. For this reason, we developed a spectrally resolved ARS set-up.

V SPECTRALLY RESOLVED ARS SET-UP

Last facility involved at the lab is a ARS set-up which allows to choose the illumination wavelength. The system uses a super continuum laser as a source. Its emission spectrum is given Figure 19. As shown Figure 20, a spectral splitter and a double monochromator are added to the super-continuum laser in order to get an illumination source with a 0.5 nm spectral

bandwidth and a tunable central wavelength on the range [480nm -2000 nm]. Moreover the use of remoted density allows an automatic tuning of the incident power on the component.

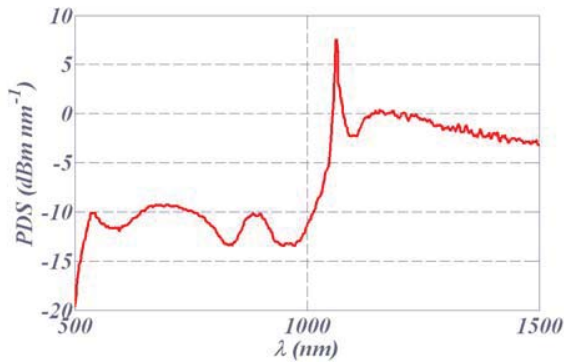


Figure 19: Emission spectrum of the super-continuum laser used as illumination source. The spectrum was recorded at t10% of maximum power available.

The set up is detailed Figure 20. The sample is illuminated using an achromatic collimator and the light scattered by the component is collected by the symmetric achromatic collimator. Then, the collected light is sent to the sensor through an optical fiber and a secondary imaging system which will image the interface of the collection fiber on a high sensitivity CCD array.

An important thing to notice here is that the use of a high power source and a high sensitivity CCD-array allow the recording of low level intensities, so the recording of scattering patterns. And, on the other hand, the presence of remoted optical densities allows the measurement of high level intensities, so the recording of specular and direct beams is made possible. For these reasons, measurements can be performed with more than 12 decades of dynamic.

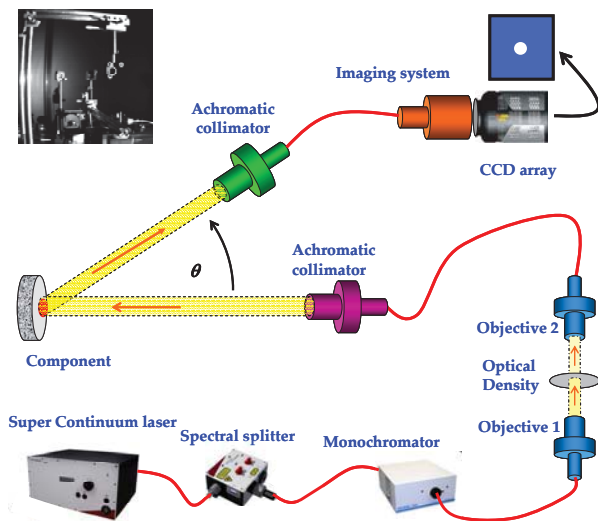


Figure 20: schematic view of the spectrally resolved ARS set-up

The calibration of the set up is performed with the measurement of a perfect diffuser (following a lambertian law), the resulting recorded pattern and the instrument signature are given Figure 21 for a 600 nm illumination wavelength.

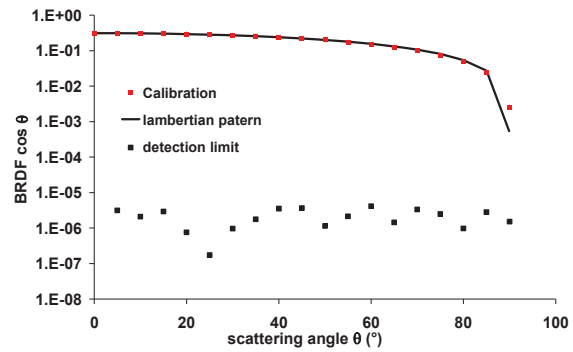


Figure 21: calibration pattern and instrument signature of the spectrally resolved ARS set-up @ λ = 600 nm

An example of application is given Figure 22 where we can see the measurement performed on a complex optical filter. The ARS patterns were recorded for three different illumination wavelengths: λ = 641 nm, λ = 740 nm, λ = 840 nm and for the two first wavelengths, the presence of scattering rings can be noticed.

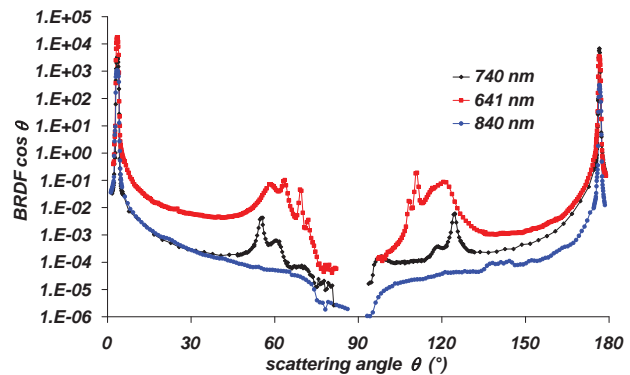


Figure 22: BRDF patterns recorded on a complex optical filter @ λ = 641 nm, λ = 740 nm, λ = 840 nm.

CONCLUSION

The increasing complexity of thin film coatings generates new problematics in light scattering phenomena. To face these challenges, new facilities and modelization tools were involved at Institut Fresnel in the last few years and were presented in this paper. Numerical results illustrate the fact that numerous parameters have to be taken into account for a comprehensive light scattering characterization of optical components. But, in term of experiment, they cannot be considered with the same accuracy at the same time, so it has been necessary to involve new facilities which now constitute a metrological platform dedicated to light scattering characterization. At last, this platform was designed for the characterization of optical component, so metrological specifications are drastic but it can

also be extended to other fields of application such as biological tissues, microcavities and lighting ...

REFERENCES

- [1]. C. Amra, "Light scattering from multilayer optics. II. Application to experiment," *J. Opt. Soc. Am. A* 11(1), 211 (1994).
- [2]. C. Amra, "Light scattering from multilayer optics. I. Tools of investigation," *J. Opt. Soc. Am. A* 11(1), 197 (1994).
- [3]. C. Amra, C. Grezes-Besset, and L. Bruel "Comparison of surface and bulk scattering in optical multilayers", *Appl. Opt.* 32, 5492- (1993)
- [4]. J. M. Bennett and L. Mattsson, *Introduction to Surface Roughness and Scattering*, 2nd ed (OSA, Washington, DC, , 1999).
- [5]. A. Duparre, B. J. Ferre, S. Gliech, G. Notni, J. Steinert, and J. M. Bennett, "Surface characterization techniques for determining the root-mean-square roughness and power spectral densities of optical components," *Applied Optics* (2002).
- [6]. P. Roche and E. Pelletier, "Characterizations of optical surfaces by measurement of scattering distribution," *Appl. Opt.* 23(20), 3561-3566 (1984).
- [7]. J. C. Stover, *Optical Scattering: Measurement and Analysis*, 2nd ed., Scatter, Measurements and Instrumentation, (SPIE, Bellingham WA, (Chapter 6). 1995).
- [8]. J. Sorrentini, M. Zerrad, and C. Amra, « Statistical signatures of random media and their correlation to polarization properties », *Opt. Lett.* 34, 2429-2431 (2009)
- [9]. O. Gilbert, C. Deumié, and C. Amra, "Angle-resolved ellipsometry of scattering patterns from arbitrary surfaces and bulks", *Opt. Express* 13, 2403-2418 (2005)
- [10]. S. Maure, G. Albrand, and C. Amra, "Low-level scattering and localized defects," *Appl. Opt.* 35(28), 5573-5582 (1996).
- [11]. M. Zerrad, C. Deumié, M. Lequime, and C. Amra, "An alternative scattering method to characterize surface roughness from transparent substrates," *Opt. Express* 15(15), 9222-9231 (2007).
- [12]. M. Lequime, M. Zerrad, C. Deumie, C. Amra, "A goniometric light scattering instrument with high-resolution imaging," *Optics Communications* 282, 1265-1273 (2009).
- [13]. M. Zerrad, M. Lequime, C. Deumie, and C. Amra, "Characterization of Optical Coatings with a CCD Angular and Spatial Resolved Scatterometer," presented at the *Optical Interference Coatings*, 2007.
- [14]. M. Zerrad, M. Lequime, C. Deumie, and C. Amra, "Development of a goniometric light scatter instrument with sample imaging ability," presented at the *SPIE Europe Optical Systems Design (Invited Paper)*, Glasgow, Scotland, 2-5th september 2008/, 2008.
- [15]. M.Zerrad, M. Lequime et al. "CCD-ARS set-up: a comprehensive and fast high-sensitivity characterisation tool for optical components" *SPIE Photonics Europe*, 2010 - Vol. 7718
- [16]. M. Zerrad, M. Lequime, C. Amra, "Multimodal high-sensitivity ARS set-up" *Multimodal high-sensitivity ARS set-up" Optical Fabrication, Testing, and Metrology IV at SPIE Europe Optical Systems Design*, Marseille, France 2011, invited paper
- [17]. M. Zerrad and M. Lequime "Instantaneous spatially resolved acquisition of polarimetric and angular scattering properties in optical coatings", *Appl. Opt.* 50, C217-C221 (2011)